Theor Chem Acc (2009) 123:455–468
DOI 10.1007/s00214-009-0557-5

REGULAR ARTICLE

DNA bindings of a novel anticancer drug, *trans*-[$PtCl_2$(isopropylamine)(3-picoline)], and kinetic competition of purine bases with protein residues in the bifunctional substitutions: a theoretical DFT study

Yan Gao · Lixin Zhou

Received: 19 November 2008 / Accepted: 10 March 2009 / Published online: 8 April 2009

Abstract The coordination of an activated novel anticancer drug, *trans*-[$PtCl_2$(ipa)(3-pico)] (ipa = isopropylamine, 3-pico = 3-methylpyridine), to DNA in a two-step process has been studied using a combination of DFT theory and IEF–PCM approach. The computed free energy barrier for the first substitution is 16.9/16.9 kcal/mol for *trans*-Pt-chloroaqua → *trans*-/*cis*-Pt–guanine monoadduct, 18.7/18.7 kcal/mol for *trans*-Pt-chloroaqua → *trans*-/*cis*-Pt–adenine monoadduct. Barriers of 20.2/20.2 kcal/mol are evaluated for *trans*-Pt-diaqua → *trans*-/*cis*-Pt–guanine monoadduct, 26.0/26.0 kcal/mol for *trans*-Pt-diaqua → *trans*-/*cis*-Pt–adenine monoadduct. In the second substitution starting from *trans*-Pt–guanine monoadduct to *trans*-diadducts, the reaction barrier for (G–Pt–G) head-to-head formation is 22.2 kcal/mol, while 22.0 kcal/mol is evaluated for the head-to-tail configuration. Barriers for (A–Pt–G) head-to-head and head-to-tail formation are 25.7/28.9 kcal/mol, respectively. The observed preference for guanine is explained in terms of remarkable larger complexation energy for the initial reactant complex as well as the lower barrier height for the substitutions. In the competition reactions, cysteine residue stabilizes the transition state ($\Delta G_{aq/ZPE}$ = 13.1 kcal/mol) for platination more efficiently than purine bases and other protein residues.

Keywords *Trans*-[$PtCl_2$(isopropylamine)(3-picoline)] · DFT · Transition state · Protein residues · Purine bases

1 Introduction

Cisplatin is a potent anticancer drug that is widely used for testicular, ovarian, head, neck and small cell lung cancers. The primary target of cisplatin is genomic DNA, specifically the N7 position of guanine bases. This point of attack first generates monofunctional adducts, which subsequently closes by coordination to the N7 position of another purine to afford didentate [1, 2]. The most notable ones are the intrastrand didentate adducts 1,2-d(GpG) at ~65% of the total amount of adducts, and 1,2-d(ApG) at ~25% [3, 4]. These adducts have also been pointed out as the ones correlating to the anticancer properties of cisplatin since they are not formed by the clinically inactive geometric isomer transplatin [5], although this view is not unchallenged. Other adducts formed are the intrastrand 1,3-d(GpNpG) (N being any base), the interstrand GG adduct, monofunctional adducts to guanine, and various DNA protein adducts [6, 7]. Although cisplatin was FDA approved in 1978 and is one of the most successful anticancer drugs, side effects, natural and acquired resistance of patients toward the drug and its limited scope have motivated searches for structurally and/or functionally analogous alternatives [8]. These effects include functionalization of ligands and the *trans*-geometry platinum.

Its direct *trans* isomer, transplatin has been confirmed to be clinically inefficient due to its inability (or bad ability) to bind to adjacent nucleobases on the same DNA strand [9, 10]. Also, transplatin forms likewise pretty few interstrand cross-links (CLs) [10]. The reason for the few amount of intrastrand CLs is the steric hindrance which does not exist

Electronic supplementary material The online version of this article (doi:10.1007/s00214-009-0557-5) contains supplementary material, which is available to authorized users.

Y. Gao · L. Zhou (✉)
Department of Chemistry, Jinan University,
510632 Guangzhou, Guangdong,
People's Republic of China
e-mail: tlzhou@jnu.edu.cn

in cisplatin, while the low efficiency of interstrand CLs should be due to the slow transformation of the monoadducts to didentates, which affords enough time for inactivation of monoadducts by intracellular sulfur-containing nucleophiles. Hence, a tactic to activate the *trans*-geometric platinum includes chemical modifications which could enhance the stability of intrastrand CLs in double-strand DNA and/or increase the rate of the formation of the interstrand CLs.

Various kinds of "nonclassical" *trans*-platinum complexes owning antitumor activity have been proposed and described [9, 11, 12]. Generally, the cytotoxicity of all *trans*-platinum complexes examined is greater than that of transplatin and they are at least as cytotoxic as their direct *cis*-isomers [13]. Additionally, *trans*-platinum complexes containing planar amines exhibit in vitro cytotoxicity equivalent to cisplatin in many human tumor cell lines.

Although the anticancer activity and properties of *trans* platinum(II) have been presented [9, 14–18], comprehensive theoretical descriptions of the DNA-binding of these agents are scarce. Herein, a DFT study of the DNA-binding properties of an activated novel *trans* platinum(II) anticancer drug, *trans*-[$PtCl_2$(ipa)(3-pico)], is carried out.

We selected 3-methylpyridine (3-pico) and isopropylamine (ipa) as ligands because Ramos-Lima et al. [11] reported that the replacement of both ammine ligands in transplatin by one aliphatic and one planar heterocyclic ligand generated new cytotoxic platinum compounds exhibiting markedly enhanced activity in cancer cell lines compared to parent transplatin or other transplatin analogues with two ligands either heterocyclic or aliphatic amine ligands. Furthermore, transplatin analogues in which both ammine ligands are replaced by a heterocyclic and an aliphatic amine ligand, respectively, form more bifunctional adducts than the parent transplatin, although slightly less than cisplatin. Additionally, monofunctional adducts of transplatin analogues close to become bifunctional adducts with a considerably higher rate than monofunctional adducts of parent transplatin forming bifunctional adducts [9]. Among these, *trans* platinum compounds with either isopropylamine or 3-picoline are most frequently studied. Transplatin analogues containing isopropylamine ligand are examined to exhibit a cytotoxic activity in cisplatin sensitive cells comparable to that of cisplatin [19] have IC50 values lower than that of cisplatin [20] or readily to form interstrand cross links in double-strand DNA [21]. On the other hand, complexes of the type *trans*-[$PtCl_2NH_3$(L)] (L = pyridine, picoline, etc.), containing a sterically demanding planar amine, exhibit increased cytotoxicity compared to the parent transplatin [22–24]. Thus, we carried out this theoretical computation to evaluate whether the combination of isopropylamine and 3-picoline ligands leads to promoted cytostatic effects for the *trans* platinum agents.

As mentioned above, for the Pt anticancer drug it is generally established that the major target leading to cell death is genomic DNA. In this paper, binding modes include monofunctional binding to a single purine base (Scheme 1), inter-/intra-strand bifunctional binding and DNA–protein cross-linking. We employ small models excluding the sugar-phosphate backbone; only the moieties directly involved in the substitution are included in each reaction step.

The chloro form of the *trans* platinum cannot react with bio-cellular directly; prior to its attack on them, one or both chlorides are substituted by water molecular, generating positively charged species. This occurs when *trans* platinum passes from the relatively high chloride concentration of the blood plasma to the lower concentration of the cell cytoplasm. A detailed discussion for the hydrolysis processes of *trans*-[$PtCl_2$(ipa)(3-pico)] is in our previous paper [25].

The most common view is that only one chloride is hydrolyzed before the attack on DNA [26]. Yet the conflicting view [27] points out that the ratio of 1,2-d(ApG) to 1,2-d(GpG) adducts found in vivo studies (ratio 1:3) of cisplatin–DNA bond formation as being better reproduced

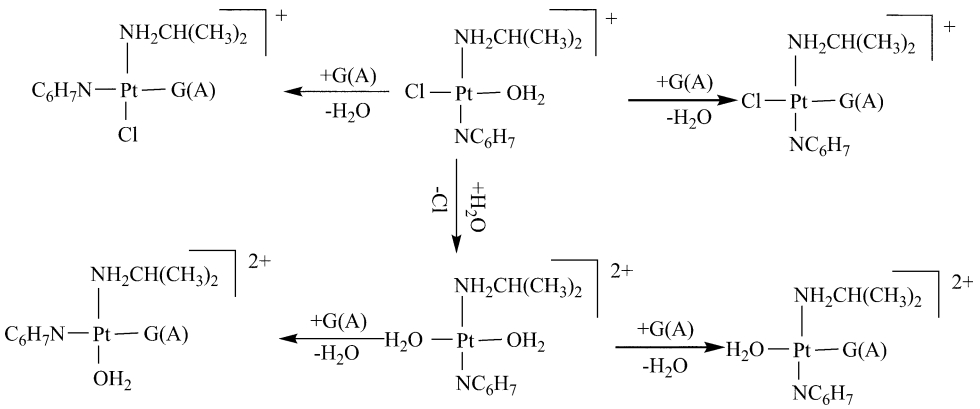

Scheme 1 Reaction paths starting from the *trans*-RC to the *trans*- or *cis*-PC in the present work

by exposure to diaquated than monoaquated cisplatin. Since it is currently not established whether the chloroaqua or diaqua complex or both of them act as the active species for the monofunctional substitution, we carried out two series of calculations using both of them as reactants. When the water is released from the Pt moiety, we adopted two possible orientations in the product complexes. In the first orientation the released water forms H-bonds with the purine base and in the alternative structure the released water points to the remaining chloride/water ligand. Two kinds of transition state structures were also computed corresponding to the product complexes.

On the other hand, it is possible that the *trans*-geometric reactant complex (RC) may generate *trans*- or *cis*-geometric product complex (PC) via the same or very similar transition state. Thus we carried out both of the reactions starting from the *trans*-RC to the *trans*- or *cis*-PC in the present work (Scheme 1). The *cis*-geometry monoadduct can then bifunctionally bind to DNA in the similar or same way with cisplain. Structures obtained through DFT calculations are presented herein to show the geometry of *trans* platinum substituted by the purines and estimates of reaction energy profiles are also displayed in the figures. The reaction barriers suggest that chloroaqua complexes are preferred over diaqua complexes with lower barrier heights.

Two patterns of cisplatin–DNA didentates have been observed experimentally for the bifunctional substitution, namely, the head-to-head (HH) in which both O6/N6 of the nucleotides are located on the same side of the platinum coordination plane, and head-to-tail (HT) configurations wherein they reside on opposite sides of the plane. The HH arrangement is observed for the intrastrand bifunctional adducts, while the HT arrangement corresponds to the interstrand adducts. We computed both isomers of product complexes in each reaction with the aim of finding the favorable geometries. Kasparkova et al. [9] have already observed the frequency of intra-/inter-strand CL for several transplatin analogues and compared that with cisplatin and transplatin. Herein, we evaluated the kinetic facets of the intra-/inter-strand CL and gave the reaction barriers for them.

Although attack on DNA is responsible for their anticancer activity, platinum drugs can interact with many other biomolecules. As a "soft" metalion Pt has a very high affinity for "soft" ligand atoms such as sulfur. Sulfur-containing biomolecules, including amino acids such as L-cysteine and L-methionine, cysteine-rich proteins such as metallothionein, are thus likely to be crucial in the metabolism of platinum drugs. Even after platinum binds to DNA, the monoadducts may interact with various compounds including sulfur-containing molecules [28]. Fojo et al. [29] reported that some of the transplanaramine (TPA) compounds displayed unusual biological profiles, the most striking of which is the production of single-stranded protein-associated DNA strand breaks and induction of DNA-topoisomerase I complexes in human tumor cells [30]. Cellular studies have further confirmed intracellular production of a higher percentage of DNA–protein CLs in comparison to cisplatin [30]. In a word, the competition reactions between DNA and protein are worth studying. In this work we present a study aiming to elucidate the competition reactions of purines and protein residues in the bifunctional substitutions. We employed four protein residues as competition ligands against purines, that is, propylamine (lysine residue), imidazole (histidine residue), mercaptomethane (cysteine residue) and dimethyl sulfur (methionine residue).

2 Computational details

All of the initial reactants were firstly optimized and calculations were carried out using density functional theory (DFT) [31]. Geometry optimizations were done in the gas phase using the Becke three-parameter hybrid exchange functional (B3) [32] and the Lee et al. [33] correlation functional (LYP) together with the LanL2DZ [34–36] effective core potential basis set for the platinum atom, while other atoms with the 6-31G(d,p) [37, 38] Pople basis set.

The optimization was then followed and verified by the vibration frequency calculations that were carried out using the same level. Transition states were conformed by intrinsic reaction coordinate (IRC) [39, 40] calculations following standard geometry optimizations and frequency calculations. Thermal energy contributions were extracted from the frequency calculations to obtain the relative Gibbs free energies at 298 K. The energies were reevaluated by additional single-point (sp) calculations on each optimized stationary point state. Single-point energy calculations were performed at the B3LYP level with the basis set of Lanl2DZ for Pt and the basis set combination 6-311 ++G (2d, 2p) [41] for other atoms. In order to incorporate the solvent effect, a family of the self-consistent reaction field (SCRF) method [42–46] has been devised for calculating systems in aqueous solution, by means of sp calculations on all stationary structures using the iso-electric focusing polarized continuum model (IEF–PCM) solution model [47–49]. The dielectric constant of water ($\varepsilon = 78.39$) was used to approximate the bulk effects of solution.

In the mono- and bifunctional substitution reactions, counterpoise (CP) method of Boys and Bernatdi [50, 51] were used on the reactant complexes to find an estimate of the basis set superposition error (BSSE), ΔE_{CP}. The obtained BSSE value was then used to calculate

complexation energies for the gas phase according to the following formula:

$$\Delta E_{\text{complexation}} = E_{\text{RC}} - E_{\text{Pt}} - E_{\text{purine}} + \Delta E_{\text{cp}}.$$

All calculations are performed using the Gaussian03 program package [52].

3 Results and discussion

The stationary points obtained are in the absence of the surrounding DNA bases and backbone, and it is therefore likely that the absolute energies obtained may deviate slightly from the actual case, that is, steric effects and the effects of the phosphoribose bridges are not included. However, considering the large similarities of the stationary point geometries it is reasonable to assume that these effects are similar in magnitude for the reaction paths studied here.

3.1 The first substitutions

Since it is currently not established whether the chloroaqua or diaqua complex or both act as the active species in the monofunctional substitutions, both of them are employed as reactants with the substituent of guanine (G) or adenine (A), generating *trans*- or *cis*-geometry product complexes. The denomination for the partaking ligands is as follows: N7 for the binding atom of the attacking purine, O6/N6 for the group that is H-bonded to Pt moiety, W_L for the leaving water ligand, and W_R for the remaining water ligand.

3.1.1 *Activated trans Pt → trans-monoadduct (trans-RC → trans-PC)*

Despite the established theory that Pt–N7 forms during the initial attack, the exact structures of the monofunctional adducts are unknown. Thus two possible product complexes generated by the reactant complexes proceeding via different transition states are included in each reaction, labeled as PC1/TS1 and PC2/TS2, respectively.

The naming convention for the optimized stationary points is (ClG, ClA, WG, WA)·(RC, TS, PC), for example, the chloroaqua reactant complex for the reaction wherein the substituent is guanine is donated ClG·RC; the corresponding product complexes are ClG·PC1/ClG·PC2; and the diaqua reactant complex relative to guanine is donated WG·RC.

The partaking complexes are fully optimized on the basis of the established Pt binding to N7 theory during the initial attack. The optimized structures of RC, TS, PC for the reaction starting from Pt-chloroaqua to *trans*-Pt–G monoadducts are schematically illustrated in Fig. 1 to show the reaction processes. Other optimized structures as well as key geometry parameters are displayed in Figure S1. The absolute energies of distinct structures for chloroaqua and diaqua complexes are listed in Table 1. Cartesians coordinate and vibrational frequencies for all optimized structures in this work are available in Tables S4 and S5. "tt" stands for the *trans*-RC → *trans*-PC reactions computed in this subsection.

The hydrogen-bond donors of activated *trans* platinum enable the drug to form stable complexes through

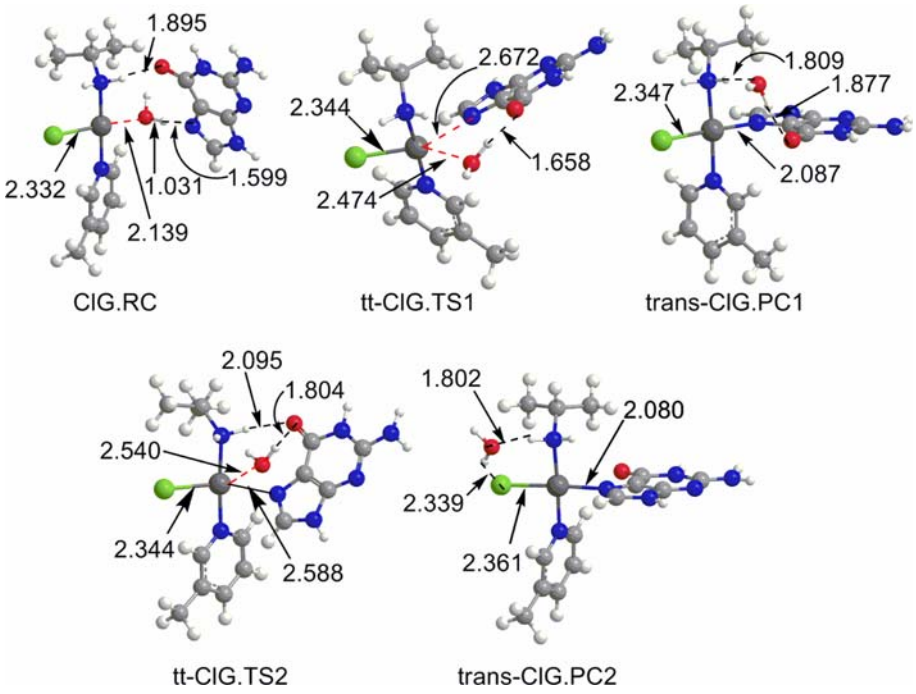

Fig. 1 Optimized structures for reaction starting from Pt-chloroaqua to *trans* Pt–G monoadducts

Table 1 Energy components for the first substitution of *trans*-Pt chloroaqua/diaqua → *trans*-monoadduct with guanine (G) or adenine (A)

State	ZPE[a]	E^a	H^a	G^a	$E_g{}^b$	$G_{aq}{}^c$
ClA·RC	0.385952	−1584.737116	−1584.736171	−1584.824090	−1585.481528	−1585.540180
tt-ClA·TS1	0.385527	−1584.702474	−1584.701530	−1584.787263	−1585.447006	−1585.507975
tt-ClA·TS2	0.385092	−1584.704796	−1584.703852	−1584.791388	−1585.449372	−1585.509520
trans-ClA·PC1	0.386100	−1584.746790	−1584.745846	−1584.832848	−1585.496525	−1585.554319
trans-ClA·PC2	0.385192	−1584.746615	−1584.745671	−1584.834103	−1585.495663	−1585.554528
ClG·RC	0.390576	−1659.990926	−1659.989982	−1660.080838	−1660.770636	−1660.831911
tt-ClG·TS1	0.389322	−1659.957839	−1659.956895	−1660.046565	−1660.736967	−1660.803712
tt-ClG·TS2	0.389750	−1659.959178	−1659.958234	−1660.047541	−1660.737396	−1660.800497
trans-ClG·PC1	0.389995	−1659.991572	−1659.990628	−1660.081735	−1660.775023	−1660.840747
trans-ClG·PC2	0.389679	−1659.990960	−1659.990016	−1660.080909	−1660.774081	−1660.841894
WA·RC	0.411667	−1200.602102	−1200.601157	−1200.689634	−1201.362124	−1201.582908
tt-WA·TS1	0.409459	−1200.549353	−1200.548409	−1200.634922	−1201.304734	−1201.539212
tt-WA·TS2	0.409730	−1200.549167	−1200.548223	−1200.634346	−1201.304662	−1201.535708
trans-WA·PC1	0.409487	−1200.601283	−1200.600339	−1200.689803	−1201.365809	−1201.589574
trans-WA·PC2	0.410556	−1200.614339	−1200.613395	−1200.701137	−1201.376432	−1201.600826
WG·RC	0.414459	−1275.863930	−1275.862986	−1275.955752	−1276.657935	−1276.870388
tt-WG·TS1	0.414060	−1275.825411	−1275.824466	−1275.913883	−1276.615857	−1276.837846
tt-WG·TS2	0.415029	−1275.825228	−1275.824284	−1275.911957	−1276.614826	−1276.830780
trans-WG·PC1	0.414896	−1275.862510	−1275.861565	−1275.952459	−1276.660316	−1276.880330
trans-WG·PC2	0.415578	−1275.874770	−1275.873826	−1275.963714	−1276.670399	−1276.889829

The suffix g and aq means gas phase and aqua solution phase, respectively. All energy values in au

[a] Calculated values at the B3LYP/(LanL2DZ + 6-31G(d,p)) level

[b] Single-point energies at the B3LYP/(LanL2DZ + 6-311 ++G(2d,2p)) level

[c] Free energies computed in the aqueous solution phase at the B3LYP/(LanL2DZ + 6-311 ++G(2d,2p)) level

interactions with the hydrogen-bond acceptors of the purine bases exposed in the major groove of DNA, i.e., the purine N7 and the O6/N6 amine groups. Hydrogen bonds are formed from the leaving water ligand to N7 as well as from ammine ligand to O6/N6 in all RC. The O6···H bond (∼1.9 Å) in ClG·RC and WG·RC is shorter than N6···H bond (∼2.3 Å) in ClA·RC and WA·RC, which is to be expected given the stronger electronic-donating ability of O6. Proton transfers are observed from the leaving water ligand to N7 for all RC, while WG·RC displays a full proton transfer. Moreover, the diaqua complexes give rise to stronger proton transfers than the chloroaqua. It is likely because the +2 charged Pt^{2+} has stronger affinity to the water–oxygen atom, making the protons of the water ligands more cationic than the +1 charged *trans* platinum. The proton transfers result in modifications in the geometric structures of the partaking components. The largest changes are found for the Pt-moiety where the distances between the deprotonated water and the platinum are reduced (by 0.05–0.07 Å) for the reactants complexes compared to the isolated reactants. Consequently the lengths of the *trans* positioned Pt-Cl/W_R bonds are increased and this, according to the *trans*-effect theory, is a reflection of the enhanced electron-donating ability of the deprotonated water ligand. Hydrogen bonding, as we know, plays a crucial role in the stabilization of complexes. To compare the stability of Pt–G and Pt–A reactant complex, complexation energies (Table S1) are calculated using the above-mentioned method. The complexation energies of the reactant complexes for guanine and adenine reveal that these are not equally stable. This is to be expected given that the hydrogen bonds formed between the different groups are not of equal strength. In these complexes the strong electrostatic attraction enhances the binding interaction and contributes to the energetics of interactions between purine bases and platinum(II). The stronger the hydrogen bonding is, the more stable the reactant complex is. The complexations are all exothermic and the exothermicity is in favor of guanine over adenine purine.

As mentioned above, two possible product complexes, PC1 and PC2, are calculated wherein two patterns of H-bonds are found. In PC1, H-bonds are formed from the replaced water to O6/N6 and from ammine ligand to the replaced water. In PC2, the released water not only allows for the formation of an H-bond with the ammine-H but also contact with the remaining chloride/water ligand. The stronger nucleophilicity of the oxo group than the amino

group is reflected in the shorter O6···H bonds in guanine–platination than the N6···H bonds in adenine–platination. The H-bonds lead to significant geometric differences between the PCs. For instance, the Cl···H interactions in PC2 lead to longer Pt–Cl bond lengths compared with PC1 for chloroaqua complexes; and the $W_R \cdots W_L$ interactions in PC2 result in shorter $Pt-O_R$ (R = remaining) bond lengths compared with PC1 for diaqua complexes.

Analysis of the constituent energy contributions to the energy difference for the isomers revealed two main contributions: solvation and electronic energy. Hydrogen bonds have been implicated to impose not only structural but also kinetic [53–55] control on the stabilization of the complexes, yet addition of solvation energies result in significant corrections to the reaction energies in both absolute numbers and the relative ordering. Overall, the substitution is accompanied with a significant loss of solvation energy while the H-bond contributes to the electrostatic energy. A convincing example of how these two effects determine the overall stability can be obtained by comparing the isomers, e.g., ClG·PC1 versus ClG·PC2. In ClG·PC2 where the released water is positioned to avoid a hydrogen bond to the guanine-O6, the strong O6···H hydrogen bond is lost. Yet the electrostatic interaction between the chloride ligand and the released water-H gives rise to some compensation, thus resulting in only a 0.6 kcal/mol preference for ClG·PC1 over ClG·PC2. Addition of solvation energy overturns the preference to ClG·PC2 by 0.7 kcal/mol (Table 1, G_{aq}). It is important that we consider differential solvation energies here because interactions with solvent water may stabilize ClG·PC2, where fragments (specifically the guanine-O6 group) that are involved in less H-bonds than ClG·PC1 may interact more strongly with solvents to give a lower overall energy. However, we must not overinterpret this approximate approach to include solvation effects for some reasons. The first one is general reservations about how accurate the continuum models reproduce solvation effects are. The second one is that in reality, many atoms of the purine bases are not solvent accessible because they are buried in the DNA duplex, but our model places the entire fragment in a continuum solvation field. Yet we can see that whether we consider the solvation effects or not, the difference between the two isomers is small. In fact, the thermodynamic differences between the corresponding isomers are so small that which isomer is preferred is determined by the kinetic facet instead of the thermodynamic (see below). Energy components for other product complexes are listed in Table 1 and will not be given more discussions.

As for the transition states, there are so many geometrical similarities among different transition states, which is to be expected since the partaking ligands on the equatorial plane are much alike, that is, the leaving ligand (water), the entering ligand (purine), and the remaining ligand (chloride or water). All TSs display familiar trigonal–bipyramids with the equatorial ligands and platinum forming a plane and the angles between entering and leaving ligand (N7–Pt–O) are in the range of 71°–79°, yet the plane is not completely vertical with the axis line but a little skewed, indicating a distorted trigonal bipyramid. H-bonds between O6/N6 and the leaving water are observed in all TS structures. The H-bonds do not significantly alter the C–O bond length of the guanine carbonyl oxygen group which only increases from ~1.23 Å for the ClG·RC/WG·RC to ~1.24/1.26 Å for ClG·TSs/WG·TSs, and the double-bonded nature of this carbonyl oxygen is thus retained. As mentioned above, the transition states are characterized by the familiar trigonal–bipyramidal structural motif typical for an associative ligand exchange mechanism. For example, in ClG·TS1/ClG·TS2 the Pt−N7 bond formed at a distance of 2.67/2.59 Å that is approximately 0.5 Å longer than the final distance in the product complexes, while Pt–OH_2 bond is halfway broken at a distance of 2.47/2.54 Å, about 0.3 Å longer than that in the reactant complexes. Comparing the isomers, ClG·TS1 is less stable than ClG·TS2 in the gas phase maybe due to the additional ammine-H···O6 bond in the latter. When solvation energy is included, the preference turns to ClG·TS1. Energies for other TS isomers are listed in Table 1 and will not be given more discussions.

Since the PC isomers in each reaction are generated by the same reactant complex, the reaction barriers are determined only by the stabilization of the transition states; the more stable the TS is, the lower the barrier is.

In order to give a clear kinetic picture of the reaction process, the relative free energies computed in the aqueous phase including ZPE corrections ($G_{aq/ZPE} = G_{aq} + ZPE$) are displayed in Fig. 2. All substitutions are exothermic according to Fig. 2, from which we can also see that for chloroaqua complexes, the computed barrier height for ClG·PC1 formation is 16.9 kcal/mol, while 19.2 kcal/mol is calculated for ClG·PC2. 19.9 kcal/mol is evaluated for ClA·PC1, with 18.7 kcal/mol for ClA·PC2. Thereby for guanine–platination, PC1 is kinetically favored, while for adenine–platination, PC2 is kinetically favored and the exothermicity differences between corresponding isomers are very small. Consequently, we can conclude that the isomers with lower barrier height, that is, ClG·PC1 and ClA·PC2, are the preferred compounds in the reactions. For diaqua complex in Fig. 2b, activation energy is in favor of WG·PC1 and WA·PC1 for guanine and adenine, respectively, with the barrier height of 20.2 and 26.0 kcal/mol, respectively. Although WG·PC2 and WA·PC2 give rise to more reaction energies, the kinetic preference is the determining facet; therefore, WG·PC1 and WA·PC1

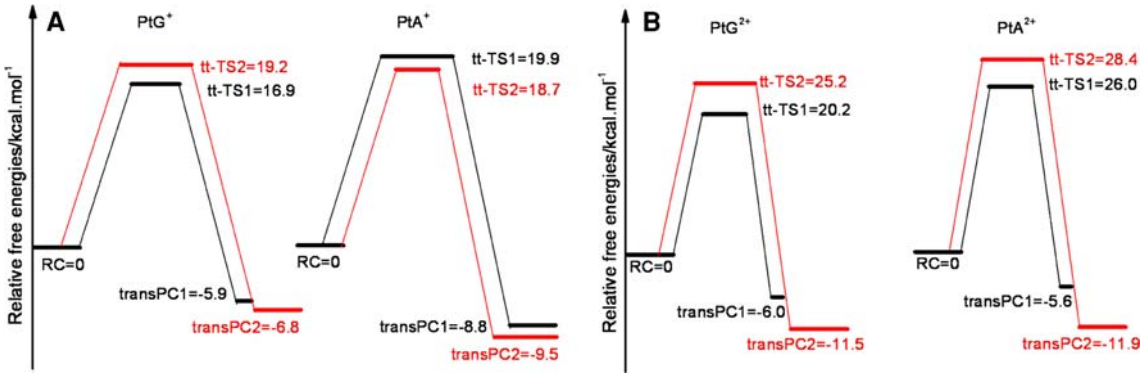

Fig. 2 ZPE-corrected relative free energies including solvation effects for the monofunctional substitution of chloroaqua (**a**) and diaqua (**b**) complexes generating *trans*-geometric product complexes

associative with lower reaction barriers are the preferred compounds in the reactions. Additionally, given the more stable initial RCs together with lower activation energies for guanine, one can conclude that *trans*-Pt prefers guanine to adenine in the first substitution.

Comparing the chloroaqua and diaqua complexes, it is obvious to find that all barrier heights relative to chloroaqua are lower than those for diaqua complexes. Additionally, our computations suggest that there is only a slight preference for guanine–platination when the chloroaqua complex is the active agent, $\Delta G_{\mathrm{ClG\cdot TS1}} = 16.9$ kcal/mol, while $\Delta G_{\mathrm{ClA\cdot TS2}} = 18.7$ kcal/mol. The choice of water as dielectric medium for the PCM calculations is somewhat problematic since the purines in the context of DNA are not fully exposed to the solvent and specific interactions of the model system with surrounding portions of DNA are not taken into account. However, assuming that the DNA surrounding of the adenine on average is the same as that of the guanine, the choice of solvation model is justified when comparing relative energies of the reactions. This reasoning also applies to the second substitution.

Comparing *trans*-[$PtCl_2$(ipa)(3-pico)] with cisplatin reported by Baik et al., we can see that the activation free energies for reactions starting from Pt-chloroaqua to Pt–G monoadduct (16.9/19.2 kcal/mol) are lower than that of cisplatin (24.5 kcal/mol) [56]. The barrier heights relative to the reaction starting from Pt-chloroaqua to Pt–A monoadducts (19.9/18.7 kcal/mol) are also lower than those of cisplatin (34.7/30.6 kcal/mol) [56]. When the diaqua Pt complex is utilized as the reactant, the reaction barrier for WG·PC1 (20.2 kcal/mol) is comparable to those of possible structures of cisplatin (19.5/21.4 kcal/mol) reported by Raber et al. [57] while platination of adenine by Pt-diaqua surpasses slightly higher reaction barrier than that of cisplatin (26.0–24.0 kcal/mol) [57]. In a word, the *trans* platinum studied in our work is comparable to cisplatin or even proceeds lower reaction barrier heights in some of the reaction processes for the first substitution.

3.1.2 *Activated trans Pt → cis-monoadduct (trans-RC → cis-PC)*

In addition to the foregoing *trans*-RC → *trans*-PC reactions (tt), it is possible that the *trans*-geometry RC can also generate *cis*-geometry PC. Thus another alignment of *trans*-RC → *cis*-PC is proposed and carried out here. Similarly, the reactant complexes generate two possible product complexes proceeding via different transition states in each reaction. The naming convention conforms with that of the tt alignment and the prefixion "tc" ("tc" stands for *trans*-RC → *cis*-PC reactions) is used for the transition states in order to distinguish with those of tt alignment.

The optimized structures of tc-TS and *cis*-PC for the reaction starting from *trans*-Pt-choroaqua complex to *cis*-Pt–G monoadduct are displayed in Fig. 3 to show the reaction processes. Other optimized structures are displayed in Figure S2 and key geometry parameters are displayed. The energy components for the chloroaqua and diaqua complexes of tc alignment are listed in Table 2. In *cis*-PC1s, H-bond patterns are similar to those for *trans*-PC1s, i.e., the released water-H is hydrogen bonded to the purine-O6/N6 group and the ammine-H is hydrogen bonded to the released water–oxo, yet difference is observed for the H-bond length for direct *trans*-/*cis*-isomers. Energy difference for most of the *cis*-/*trans*-isomers are small in the gas phase (∼2 kcal/mol or smaller than 2 kcal/mol); the exceptions are *cis*/*trans*-ClG·PC2, *cis*/*trans*-WG·PC2 and *cis*/*trans*-WA·PC2 isomers; and these differences are even smaller when solvation correction is added. For instance, the energy difference between the *cis*-/*trans*-ClG·PC1 isomers is only 1.5 kcal/mol in the gas phase (E_g). When solvation energy is added, the preference

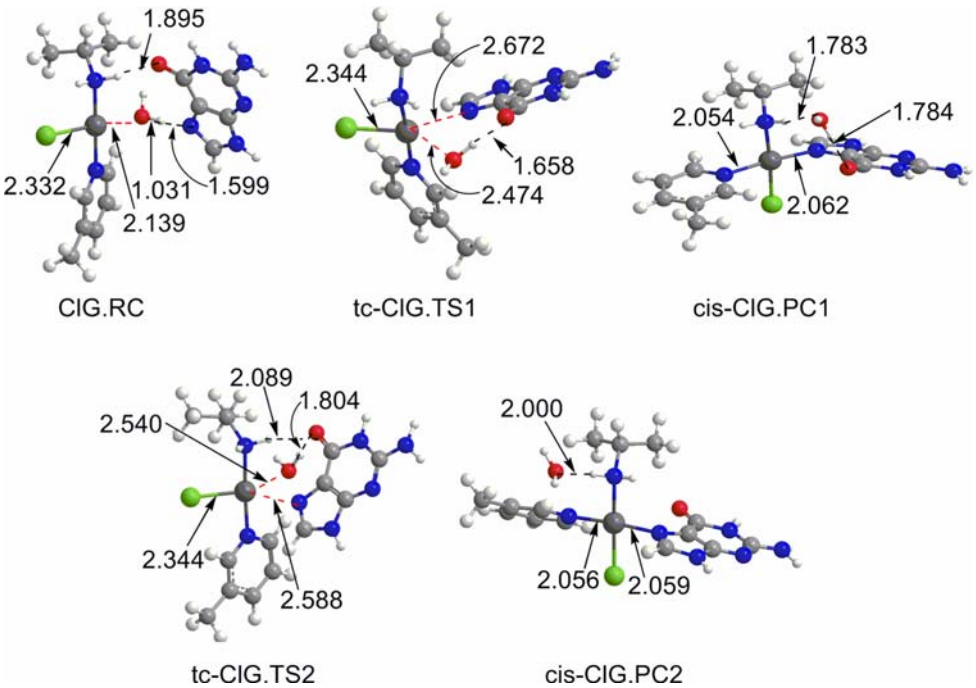

Fig. 3 Optimized structures for reaction starting from Pt-chloroaqua to *cis*-Pt–G monoadducts

Table 2 Energy components for the first substitution of *trans*-Pt chloroaqua/diaqua → *cis*-monoadduct with guanine (G) or adenine (A)

State	ZPE[a]	E^a	H^a	G^a	E_g[b]	G_{aq}[c]
tc-ClA·TS1	0.385525	−1584.702475	−1584.701531	−1584.787275	−1585.447004	−1585.507990
tc-ClA·TS2	0.385092	−1584.704796	−1584.703852	−1584.791388	−1585.449372	−1585.509520
cis-ClA·PC1	0.386321	−1584.746370	−1584.745426	−1584.832247	−1585.494525	−1585.551875
cis-ClA·PC2	0.386143	−1584.746752	−1584.745808	−1584.832983	−1585.494865	−1585.552205
tc-ClG·TS1	0.389321	−1659.957840	−1659.956896	−1660.046565	−1660.736967	−1660.803678
tc-ClG·TS2	0.389751	−1659.959178	−1659.958234	−1660.047548	−1660.737397	−1660.800556
cis-ClG·PC1	0.389920	−1659.988765	−1659.987821	−1660.080272	−1660.772664	−1660.840851
cis-ClG·PC2	0.389048	−1659.980860	−1659.979916	−1660.072719	−1660.765039	-1660.840247
tc-WA·TS1	0.409459	−1200.549353	−1200.548409	−1200.634922	−1201.304734	−1201.539212
tc-WA·TS2	0.409732	−1200.549166	−1200.548222	−1200.634344	−1201.304663	−1201.535701
cis-WA·PC1	0.409921	−1200.602481	−1200.601537	−1200.690382	−1201.365828	−1201.590970
cis-WA·PC2	0.409609	−1200.603727	−1200.602783	−1200.689332	−1201.366402	−1201.592933
tc-WG·TS1	0.414060	−1275.825411	−1275.824467	−1275.913882	−1276.615857	−1276.837845
tc-WG·TS2	0.415029	−1275.825229	−1275.824285	−1275.911960	−1276.614826	−1276.830770
cis-WG·PC1	0.415041	−1275.866693	−1275.865749	−1275.956255	−1276.663657	−1276.881464
cis-WG·PC2	0.415018	−1275.884685	−1275.883740	−1275.975258	−1276.681912	−1276.892440

The suffix g and aq means gas phase and aqua solution phase respectively. All energy values in au

[a] Calculated values at the B3LYP/(LanL2DZ + 6-31G(d,p)) level

[b] Single-point energies at the B3LYP/(LanL2DZ + 6-311 ++G(2d,2p)) level

[c] Free energies computed in the aqueous solution phase at the B3LYP/(LanL2DZ + 6-311 ++G(2d,2p)) level

inverts to *trans*-ClG·PC1 and the energy difference is even smaller.

H-bond patterns in *cis*-PC2s are more complicated. For *cis*-ClG·PC2, only one H-bond is observed, from the amine-H to the released water–oxo. Thus it is less stable than *cis*-ClG·PC1 by 4. 8 kcal/mol in the gas phase. As for *cis*-ClA·PC1 versus *cis*-ClA·PC2, due to the same H-bond pattern and similar H-bond strength, the isomers are almost isoenergetic. For *cis*-WG·PC2, one of the remaining-water-H is hydrogen bonded to the guanine-O6 group and the other is H-bonded to the released-water-oxo. These H-bonds are considerably stronger than the H-bonds in

cis-WG·PC1, thus *cis*-WG·PC2 is more stable. Turning to *cis*-WA·PC1 versus *cis*-WA·PC2, the H-bond patterns are the same and the H-bond length is similar, thus the isomers are almost isoenergetic.

The optimized TS structures of the tc alignment are very similar to the corresponding ones in tt alignment. Even the H-bond patterns and bond length are generally the same although some H-bonds length displays slight difference with the tt-TS. The structures of tc-TS are displayed in Figure S2 and will not be given more discussions. Similar structures result in very similar stabilization for transition states of both alignments. The relative energy profiles for tc alignment are displayed in Fig. 4. Comparing Fig. 4 with 2, it is not difficult to find that the reaction barriers for tc alignment are very similar to (or identical with) the corresponding values for tt alignment. The similar reaction barriers as well as the similar TS structures suggest that the *trans*-reactant complex can generate *cis*- and *trans*-geometric product complex via very similar transition states. Besides, the reaction energies in Figs. 2 and 4 show that the energy differences between direct *cis/trans*-PC isomers are even smaller than those in the gas phase. An obvious example is *cis/trans*-ClG·PC2 and *cis/trans*-WG·PC2. For the former, the energy difference is 0.6 kcal/mol in the aqua solution, smaller than 5.7 kcal/mol in the gas phase. For the latter, energy difference is 2.0 kcal/mol compared to 7.2 kcal/mol in the gas phase.

In a word, given the similar reaction barriers and reaction energies we can draw the conclusion that tc reactions are comparable to tt reactions. The *cis*-geometric products (monoadducts) can subsequently close to form the bifunctional intrastrand DNA–Pt–DNA didentates and maybe *trans* platinum can distort DNA in the similar way with cisplatin.

3.2 The second substitutions

Given the preference of guanine binding to DNA and the predominance for PC1 in the first substitution, we employed WG·P1 (which is derived from WG·PC1in tt alignment, eliminating the substituted water) as the initial reactant in the second substitution with the substituent of either purine bases or protein residues.

3.2.1 *trans Pt–G monoadduct → trans DNA–Pt–DNA diadduct*

The naming convention used for the complexes is (GG, GA)·(HH, HT)·(RC, TS, PC). For example, the reactant complex for the reaction in which the second substituent is guanine on a path leading to both of HH and HT configuration is denoted GG·RC; the product complexes are GG·HH·PC and GG·HT·PC. The optimized structures for GG·RC generating G–Pt–G diadducts are displayed in Fig. 5 as examples. Other optimized structures are shown in Figure S3.

The initial attack of purines to *trans* Pt in the second substitutions generally follows the pattern established in the first substitution, that is, N7 of the purine is hydrogen-bonded to the leaving water and O6 is hydrogen-bonded to the ammine ligand. Proton transfers are observed in both of the RCs, wherein the distances between platinum and the water ligand are 2.09 and 2.06 Å for GG·RC and GA·RC, respectively, shorter than that of WG·PC1 (2.15 Å). The shortening of the bond lengths is mainly due to the proton transfer from the water ligand to the G/A substituent, which creates more stable Pt–O covalent bond.

On visual inspection of the GG·RC and GA·RC structures, these would seem unlikely RC geometries for adjacent DNA bases located on the same strand, given that the distance between the guanine N9 atoms in our geometry, in vivo bonding to the ribose of the DNA backbone, is 10.17 and 10.58 Å, respectively. This is likely an effect of the model system not accounting for the restraints imposed by the adjoining parts of DNA. However, it must be kept in mind that the DNA molecule is very flexible and intrastrand didentate adducts are also known to be formed

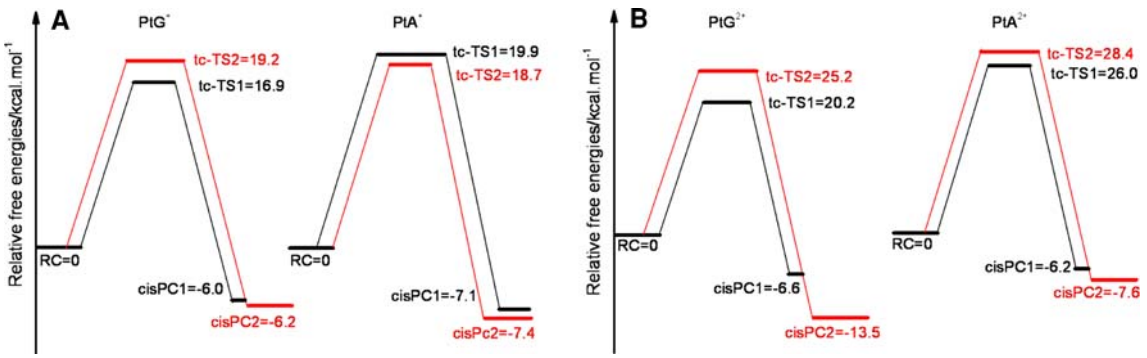

Fig. 4 ZPE-corrected relative free energies including solvation effects for the monofunctional substitution of chloroaqua (**a**) and diaqua (**b**) complexes generating *cis*-geometric product complexes

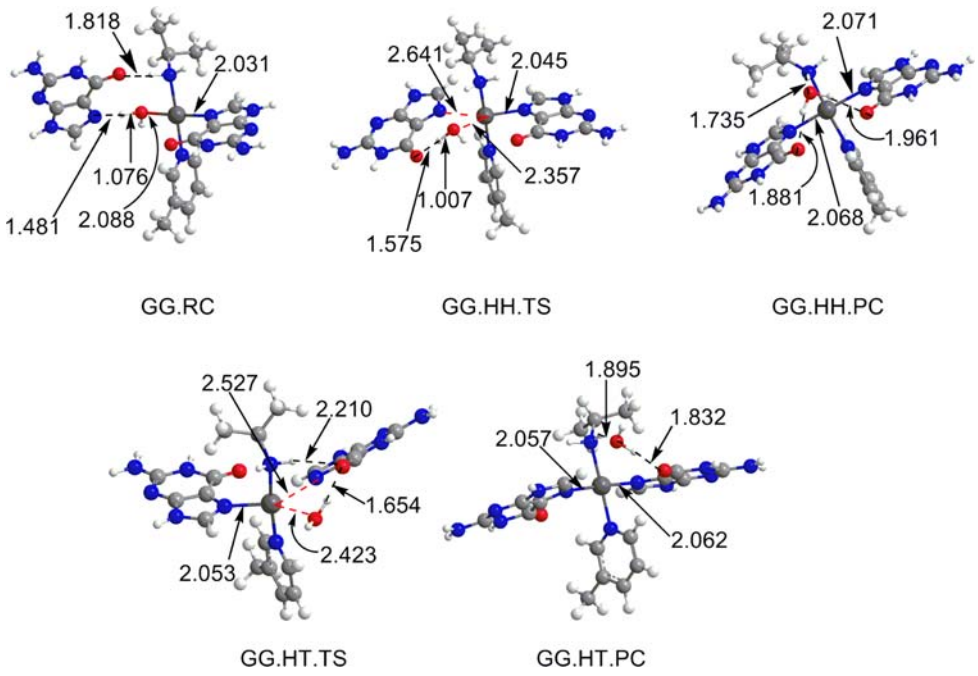

Fig. 5 Optimized structures for the bifunctional substitution of *trans* Pt–G monoadducts → *trans* G–Pt–G diadduct

between guanines separated by one nucleotide in the sequence.

Both of the HH and HT configuration product complexes have been obtained. Overall, the structures of the G–Pt–A diadducts display more standard four-square planes than G–Pt–G diadducts, in the former both of the N(ipa)–Pt–N(3-pico) angles and N7–Pt–N7 angles ranging between 177°–179° with the corresponding range of 172°–177° for the latter. These ideal four-square planes may be only observed in the theoretical computation, which is absent in the experiment due to the force exerted on the adducts by the surrounding DNA, in particular the DNA phosphoribose bridge. Hydrogen bonds in GG·HT·PC and GA·HT·PC are formed from the water-H to the second substituted purine-O6/N6 group and from the ammine-H to the water while several additional H-bonds are found for GG·HH·PC and GA·HH·PC (Figure S3).

The transition state geometries in the second substitutions are in very agreement with those in the first substitution yet with a smaller spread in the angles between the attacking purine and leaving water ligand (a spread of 75°–77° compared to 71°–80°). The distinction between TSs in the second and first substitution is that no proton transfers are observed in the former.

Energy components of the DNA–Pt–DNA second substitutions are listed in Table S2 and calculated relative free energies in the aqueous phase including the ZPE corrections are displayed in Fig. 6. From the figure it follows that the activation energy is 22.2 kcal/mol for the formation of GG·HH·PC, only ∼0.2 kcal/mol higher than GG·HT·PC and 25.7 kcal/mol for GA·HH·PC, ∼3.2 kcal/mol lower than GA·HT·PC. Reaction energies are also in favor of GG·HT path and GA·HH path, respectively.

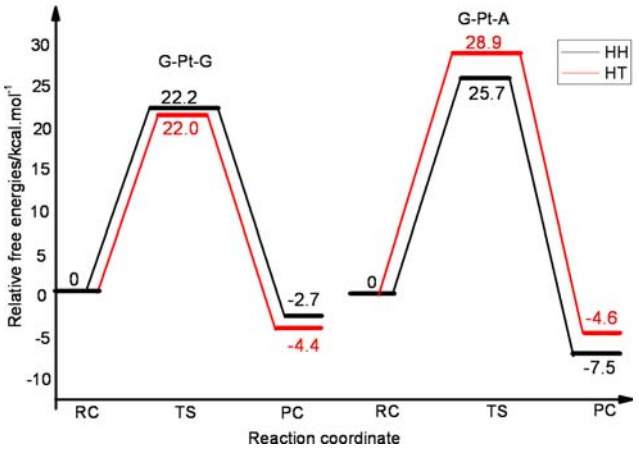

Fig. 6 ZPE-corrected relative free energies including solvation effect for the bifunctional substitution of Pt–G monoadduct with purines

Comparing inter- versus intrastrand energy profiles, the computed data suggest that for guanine interstrand adduct formation should be favored, on the basis of both the lower barriers (albeit only slightly lower) and more stable product complexes while for adenine intrastrand cross-linking is both kinetically and thermodynamically favored. Comparing the guanine and adenine substituent, guanine is obviously kinetically favored than adenine with lower barrier heights. Additionally, given the more stable reactant complexes for guanine as mentioned above, guanine has the predominance for diadduct formation over adenine.

Comparing *trans* platinum with cisplatin reported by Raber et al., we find that the G–Pt–G bifunctional substitutions of *trans*-Pt are comparable to those of cisplatin ($\Delta G_{HH\cdot PC} = 22.5$ kcal/mol and $\Delta G_{HT\cdot PC} = 21.2$ kcal/mol) [57]. However, the adenine substitution is un-comparable to that of cisplatin (25.7–21.1 kcal/mol). Taking into account the first and second substitutions of *trans* platinum with DNA, we can conclude that the replacement of the ammine ligands with a heterocyclic and an aliphatic ligand in transplatin considerably improves the action of *trans* platinum, which is generally comparable to cisplatin. Some experimental results also demonstrated that several analogues of transplatin can exhibit antitumor activity at least comparable to that of cisplatin [58].

3.2.2 *trans Pt–G monoadduct → trans DNA–Pt–protein residue CLs*

The protein residue molecules are firstly optimized and subsequently bind to the Pt–G monoadduct through S or N-atom. The water–protein residue exchanges are in good accord with the established theory for other relative substitution reactions. Naming in this subsection is as follows: L stands for lysine, H for histidine, C for cysteine, M for methionine, and (GL, GM, GC, GH)·(RC, TS, PC) for partaking complexes. Optimized structures for the substitution of P–G monoadduct with cystein residue are displayed in Fig. 7 as examples to show the reaction process. Other stationary points as well as key geometry parameters are displayed in Figure S4 and energy components are listed in Table S3.

In GL·RC and GH·RC associative to N-donors, proton transfers are observed from the water ligand to the attacking N-atom, enhancing the Pt–O covalent bond. However, in GC·RC and GM·RC where weaker H-bonds between S-atom and water ligands are found, Pt–O bond lengths are longer, demonstrating the stronger proton-affinity of N than S-atom. For product complexes, three H-bonds are found for GL·PC and GC·PC while only two are found in GH·PC and GM·PC. However, in spite of the additional H-bond in GL·PC/GC·PC, they are not electronically more preferred than other two PCs (E_g in Table S3). In the TSs with trigonal–bipyramidal structures, a hydrogen bond between the purine–O6 and ammine ligand is found for all the TSs. The N/S–Pt–O angle is between 65.6° and 69.4°, with GC·TS the smallest one probably due to the smallest bulk of cysteine that is accompanied with smallest steric repulsion.

With the aim to quantitatively evaluate the preference of the *trans* platinum to purines or protein residues, energetic terms are derived from the current calculations. The relative free energies computed in the aqueous phase including ZPE-corrections are displayed in Fig. 8. The figure shows that GC·PC is preferred for both of the lowest reaction barrier height (13.1 kcal/mol) and a relative large energy release (−11.6 kcal/mol) although it contains only one electron-donating methyl. The second lowest barrier height occurs for the substitution of methionine residue (14.9 kcal/mol) with histidine the third one (23.3 kcal/mol) and lysine the highest one (28.6 kcal/mol). The released energy is −15.7/−9.5 kcal/mol for GM·PC/GH·PC, with −5.3 kcal/mol for lysine, whose substitution is indicated to be the least favorable for both of the kinetic and thermodynamic facets. Since the more favorable cysteine and methionine residues are S-donors and the less favorable histidine and lysine residues are N-donors, we can reach the conclusion that the affinity of the S-atom to the Pt metal is higher than the N-atom. The results confirm the previously observed kinetic selectivity for sulfur over nitrogen binding [59–63].

Comparing the two S-donor substituents—cysteine versus methionine residues, the predominance for the former may be due to the weaker steric hindrance (owing to the smaller bulk of alkyl group) during the initial attack. As for histidine versus lysine residues, the stronger affinity of the former to the Pt-center may be due to the stronger electronic-donating properties of aromatic heterocycle than the alkyl group. We can see that the biologically relevant substituents, i.e., the presence of alkyl or aromatic heterocycle do have an important effect on the activation energies.

Comparing protein residues with purine bases, it shows that barrier height for G–Pt–G formation is 8 kcal/mol higher than the two S-donating protein residues. Adenine is

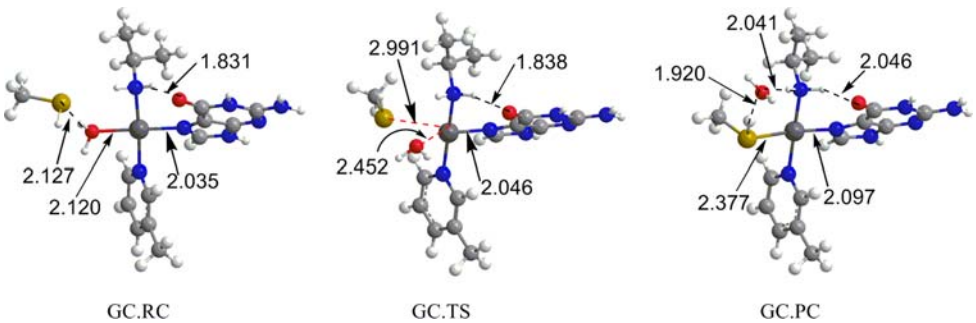

Fig. 7 Optimized structures for the bifunctional substitution of *trans* Pt-G monoadducts → *trans* G–Pt–C diadduct

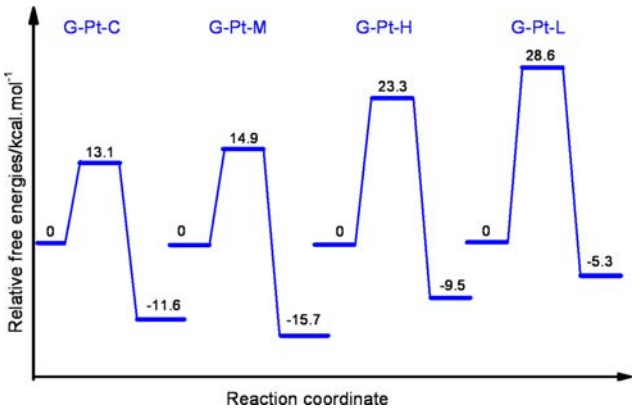

Fig. 8 Solvation and ZPE-corrected relative energies for bifunctional substitution of Pt–G monoadduct with protein residues

even less active, with higher barrier height than one of the N-donor protein residue. In a word, purine bases are kinetically un-comparable to S-containing protein residues. Model studies on the comparative kinetics of binding of methionine (model for protein) and 5′-GMP (model for DNA) to *trans*-[PtCl(9-EtGuanine)(NH_3)(quinoline)] also support the concept that protein binding is kinetically favored [64].

Although established theory suggests that cisplatin-induced DNA–DNA contribute to its cytotoxicity, biochemical studies suggest that cellular pharmacology for *trans* platinum maybe quite complex, and may involve three distinct types of DNA lesions: monofunctional adducts, bifunctional DNA–DNA CLs as well as DNA–protein CLs [65]. DNA–Pt–protein adducts for a variety of platinum complexes have been reported [65]. Although cisplatin-induced DNA–protein crosslinks appear not to contribute to cytotoxicity [53], the altered stereochemistry of transplatin analogues could increase its propensity to directly form stable links between DNA and histone or other chromatin proteins, or could make repair more difficult.

4 Conclusions

We have in this paper performed a theoretical study of the two sequential substitution reactions of a novel activated anticancer drug, *trans*-[$PtCl_2$(ipa)(3-pico)], with DNA purines and competitive reactions of DNA purine bases with protein residues in the bifunctional substitutions.

In the monofunctional substitutions using both of the chloroaqua and diaqua complexes as active species generating *trans*-/*cis*-geometry product complexes, two possible structures of transition states corresponding to two product complexes in each reaction are obtained. The geometries of the stationary points agree with relative theoretical work and established theory for ligand substitution in square planar complexes. The reaction barriers for the chloroaqua complex are overall lower than the diaqua complex.

Comparing *trans*-[$PtCl_2$(ipa)(3-pico)] with cisplatin, the barrier heights for reaction starting from *trans*-Pt-chloroaqua to Pt–G monoadduct (16.9 kcal/mol) is lower than that of cisplatin (24.5 kcal/mol). The barrier height relative to Pt-chloroaqua → Pt–A monoadduct (18.7 kcal/mol) is also considerably lower than that of cisplatin (30.6 kcal/mol). The reaction of diaqua complex with guanine has to surpass a barrier height of 20.2 kcal/mol, which is comparable to that of cisplatin (19.5 kcal/mol). Yet platination of adenine by Pt-diaqua is slightly un-comparable to that of cisplatin (26.0–24.0 kcal/mol). In the tc alignment of reactions the obtained TS structures and activation energies reveal that *trans*-geometric RC can give rise to *cis*-geometric PC in addition to the *trans*-geometric PC, and tc alignment is both kinetically and thermodynamically comparable to tt alignment. The monoadducts can subsequently close to form bifunctional adducts and may distort DNA in the similar way with cisplatin.

Given the preference to guanine in the first substitution, the bifunctional substitution employed the product originating from the diaqua complex as the initial reactant (expel the released water). The platination of guanine is kinetically and thermodynamically preferred over adenine. On the other hand, the *trans* Pt–DNA chelate shows a slight kinetic and thermodynamic preference for HT path for guanine, while for adenine HH path is kinetically and thermodynamically favored. Compared with cisplatin, the GG·HH·PC formation for *trans*-[$PtCl_2$(ipa)(3-pico)] is comparable to that of cisplatin (22.2–22.5 kcal/mol), with a little higher value for GG·HT path (22.0–21.2 kcal/mol). One can easily see that the replacement of the ammine ligands with a heterocyclic and an aliphatic ligand in transplatin results in a considerably improved transformation rate of Pt–G interstrand monoadduct to didendate. However, the adenine substitution is still uncompetitive to that of cisplatin, with the GA·HT activation energy of 28.9 kcal/mol compared to 21.1 kcal/mol for cisplatin. Considering the mono- and bifunctional substitutions, we can conclude that transplatin analog evaluated in our work is comparable to cisplatin.

The competition reactions of purines and protein residues binding to Pt–DNA monoadducts are subsequently carried out. Reaction barriers for S-containing substituents are about 8 kcal/mol lower than the DNA purine bases. We can reach the conclusion that the affinity of the S-atom to Pt metal is stronger than the N-atom in the high dielectric constant of 78.39 of water solution. The steric and electronic properties of the substituents have an important effect on the nucleophilicity of the S/N heteroatom.

References

1. Bancroft DP, Lepre CA, Lippard SJ (1990) J Am Chem Soc 112:6860. doi:10.1021/ja00175a020
2. Sherman SE, Lippard SJ (1987) Chem Rev 87:1153. doi:10.1021/cr00081a013
3. Eastman A (1986) Biochemistry 25:3912. doi:10.1021/bi00361a026
4. Fichtinger-Schepman AMJ, van Oosterom AT, Lohman PHM, Berends F (1987) Cancer Res 47:3000
5. Lepre CA, Strothkamp KG, Lippard SJ (1987) Biochemistry 26:5651. doi:10.1021/bi00392a011
6. Jamieson ER, Lippard SJ (1999) Chem Rev 99:2467. doi:10.1021/cr980421n
7. Fichtinger-Schepman AMJ, van der Veer JL, den Hartog JHJ, Lohman PHM, Reedijk J (1985) Biochemistry 24:707. doi:10.1021/bi00324a025
8. Wong E, Giandomenico CM (1999) Chem Rev 99:2451. doi:10.1021/cr980420v
9. Kasparkova J, Marini V, Najajreh Y, Gibson D, Brabec V (2003) Biochemistry 42:6321. doi:10.1021/bi0342315
10. Boudvillain M, Dalbies R, Aussourd C, Leng M (1995) Nucleic Acids Res 23:2381. doi:10.1093/nar/23.13.2381
11. Ramos-Lima FJ, Vrána O, Quiroga AG, Navarro-Ranninger C, Halámiková A, Rybníčková H, Hejmalová L, Brabec V (2006) J Med Chem 49:2640. doi:10.1021/jm0602514
12. Jawbry S, Freikman I, Najajreh Y, Perez JM, Gibson DJ (2005) Inorg Biochem 99:1983. doi:10.1016/j.jinorgbio.2005.06.011
13. Farrell N, Kelland LR, Roberts JD, Beusichem MV (1992) Cancer Res 52:5065
14. Bulluss GH, Knott KM, Ma ESF, Aris SM, Alvarado E, Farrell N (2006) Inorg Chem 45:5733. doi:10.1021/ic060741m
15. McGowan G, Parsons S, Sadler PJ (2005) Inorg Chem 44:7459. doi:10.1021/ic050763t
16. Martínez A, Lorenzo J, Prieto MJ, Font-Bardia M, Solans X, Avilés FX, Moreno V (2007) Bioorg Med Chem 15:969. doi:10.1016/j.bmc.2006.10.031
17. Anzellotti A, Stefan S, Gibson D, Farrell N (2006) Inorg Chim Acta 359:3014. doi:10.1016/j.ica.2005.12.060
18. Horvath G, Premkumar T, Boztas A, Lee E, Jon S, Geckeler KE (2008) Mol Pharm 5:358. doi:10.1021/mp700144t
19. Montero EI, Diaz S, Gonzalez-Vadillo AM, Perez JM, Alonso C, Navarro-Ranninger C (1999) J Med Chem 42:4264. doi:10.1021/jm991015e
20. Murray M, Cunningam J, Parada L, Dantry F, Labowitz P, Weinberg R (1983) Cell 33:749. doi:10.1016/0092-8674(83)90017-X
21. Pèrez JM, Montero EI, Solans X, Font-Bardia M, Fuertes MA, Alonso C, Navarro-Ranninger C (2000) J Med Chem 43:2411. doi:10.1021/jm000925p
22. Beusichem MV, Farrell N (1992) Inorg Chem 31:634. doi:10.1021/ic00030a021
23. Quiroga AG, Pérez JM, Alonso C, Navarro-Ranninger C, Farrell N (2006) J Med Chem 49:224. doi:10.1021/jm050804v
24. Zou Y, Houten BV, Farrell N (1993) Biochemistry 32:9632. doi:10.1021/bi00088a015
25. Gao Y, Zhou LX (2008) Chin J Chem Phys 21:346
26. Davies MS, Berners-Price SJ, Hambley TW (2000) Inorg Chem 39:5603. doi:10.1021/ic000847w
27. Legendre F, Bas V, Kozelka J, Chottard JC (2000) Chem Eur J 6:2002. doi:10.1002/1521-3765(20000602)6:11<2002::AID-CHEM2002>3.0.CO;2-H
28. Zimmermann T, Zeizinger M, Burda JV (2005) J Inorg Biochem 99:2184. doi:10.1016/j.jinorgbio.2005.07.021
29. Fojo T, Farrell N, Ortuzar W, Tanimura H, Weinstein J, Myers TG (2005) Crit Rev Oncol Hematol 53:25. doi:10.1016/j.critrevonc.2004.09.008
30. Farrell N, Povirk LF, Dange Y, DeMasters G, Gupta MS, Kohlhagen G, Khan QA, Pommier Y, Gewirtz DA (2004) Biochem Pharmacol 68:857. doi:10.1016/j.bcp.2004.05.023
31. Hohenberg P, Kohn W (1964) Phys Rev B136:864. doi:10.1103/PhysRev.136.B864
32. Becke AD (1993) J Chem Phys 98:5648. doi:10.1063/1.464913
33. Lee C, Yang W, Parr RG (1988) Phys Rev B37:785. doi:10.1103/PhysRevB.37.785
34. Hay PJ, Wadt WR (1985) J Chem Phys 82:270. doi:10.1063/1.448799
35. Wadt WR, Hay PJ (1985) J Chem Phys 82:284. doi:10.1063/1.448800
36. Hay PJ, Wadt WR (1985) J Chem Phys 82:299. doi:10.1063/1.448975
37. Binkley JS, Pople JA, Hehre WJ (1980) J Am Chem Soc 102:939. doi:10.1021/ja00523a008
38. Hehre WJ, Ditchfield R, Pople JA (1972) J Chem Phys 56:2257. doi:10.1063/1.1677527
39. Gonzalez C, Schlegel HB (1989) J Chem Phys 90:2154. doi:10.1063/1.456010
40. Gonzalez C, Schlegel HB (1990) J Phys Chem 94:5523. doi:10.1021/j100377a021
41. McLean AD, Chandler GS (1980) J Chem Phys 72:5639. doi:10.1063/1.438980
42. Kirkwood JG (1934) J Chem Phys 2:351. doi:10.1063/1.1749489
43. Wong MW, Frish MJ, Wiberg KB (1991) J Am Chem Soc 113:4776. doi:10.1021/ja00013a010
44. Wong MW, Wiberg KB, Frish MJ (1992) J Am Chem Soc 114:523. doi:10.1021/ja00028a019
45. Wong MW, Wiberg KB, Frish MJ (1992) J Am Chem Soc 114:1645. doi:10.1021/ja00031a017
46. Onsager L (1936) J Am Chem Soc 58:1486. doi:10.1021/ja01299a050
47. Mennucci B, Tomasi J (1997) J Chem Phys 106:5151. doi:10.1063/1.473558
48. Mennucci B, Cancs E, Tomasi J (1997) J Phys Chem B 101:10506. doi:10.1021/jp971959k
49. Tomasi J, Mennucci B, Cancs E (1999) J Mol Struct Theochem 464:211. doi:10.1016/S0166-1280(98)00553-3
50. Boys SF, Bernardi F (1970) Mol Phys 19:553. doi:10.1080/00268977000101561
51. Simon J, Duran M, Dannenberg JJ (1996) J Chem Phys 105:11024. doi:10.1063/1.472902
52. Gaussian 03, revision D.01, Frisch MJ, Trucks GW, Schlegel HB, Scuseria GE, Robb MA, Cheeseman JR, Montgomery JA Jr, Vreven T, Kudin KN, Burant JC, Millam JM, Iyengar SS, Tomasi J, Barone V, Mennucci B, Cossi M, Scalmani G, Rega N, Petersson GA, Nakatsuji H, Hada M, Ehara M, Toyota K, Fukuda R, Hasegawa J, Ishida M, Nakajima T, Honda Y, Kitao O, Nakai H, Klene M, Li X, Knox JE, Hratchian HP, Cross JB, Adamo C, Jaramillo J, Gomperts R, Stratmann RE, Yazyev O, Austin AJ, Cammi R, Pomelli C, Ochterski JW, Ayala PY, Morokuma K, Voth GA, Salvador P, Dannenberg JJ, Zakrzewski VG, Dapprich S, Daniels AD, Strain MC, Farkas O, Malick DK, Rabuck AD, Raghavachari K, Foresman JB, Ortiz JV, Cui Q, Baboul AG, Clifford S, Cioslowski J, Stefanov BB, Liu G, Liashenko A, Piskorz P, Komaromi I, Martin RL, Fox DJ, Keith T, Al-Laham MA, Peng CY, Nanayakkara A, Challacombe M, Gill PMW, Johnson B, Chen W, Wong MW, Gonzalez C, Pople JA (2004) Gaussian, Inc., Wallingford CT
53. Reedijk J (2003) Proc Natl Acad Sci USA 100:3611. doi:10.1073/pnas.0737293100

54. Chval Z, Šip M (2003) Collect Czech Chem Commun 68:1105. doi:10.1135/cccc20031105
55. Reedijk J (1992) Inorg Chim Acta 200:873. doi:10.1016/S0020-1693(00)92433-2
56. Baik MH, Friesner RA, Lippard SJ (2003) J Am Chem Soc 125:14082. doi:10.1021/ja036960d
57. Raber JR, Zhu CB, Eriksson LA (2005) J Phys Chem B 109:11006. doi:10.1021/jp050057d
58. Clarke MJ, Sadler PJ (1999) In: Natile G, Coluccia M (eds) Topics in biological inorganic chemistry, metallopharmaceuticals. Springer, Berlin, p 73
59. Teuben JM, Reedijk J (2000) J Biol Inorg Chem 5:463
60. Hahn M, Kleine M, Sheldrick WS (2001) J Biol Inorg Chem 6:556. doi:10.1007/s007750100232
61. Fakih S, Munk VP, Shipman MA, Murdoch PD, Parkinson JA, Sadler PJ (2003) Eur J Inorg Chem 1206. doi:10.1002/ejic.200390156
62. Murdoch PD, Kratchowil NA, Parkinson JA, Patriarca M, Sadler PJ (1999) Angew Chem Int Ed 38:2949. doi:10.1002/(SICI)1521-3773(19991004)38:19<2949::AID-ANIE2949>3.0.CO;2-Q
63. Marchán V, Moreno V, Pedroso E, Grandas A (2001) Chem Eur J 7:808. doi:10.1002/1521-3765(20010216)7:4<808::AID-CHEM808>3.0.CO;2-6
64. Bierbach U, Farrell N (1998) J Biol Inorg Chem 3:570. doi:10.1007/s007750050270
65. Kasparkova J, Novakova O, Farrell N, Brabec V (2003) Biochemistry 42:792. doi:10.1021/bi026614t